

Constraints on Primordial-black-hole Population and Cosmic Expansion History from GWTC-3

Zu-Cheng Chen,^{1,2,*} Shen-Shi Du,³ Qing-Guo Huang,^{4,5,6,†} and Zhi-Qiang You^{1,2,‡}

¹*Department of Astronomy, Beijing Normal University, Beijing 100875, China*

²*Advanced Institute of Natural Sciences, Beijing Normal University, Zhuhai 519087, China*

³*School of Physics and Technology, Wuhan University, Wuhan, Hubei 430072, China*

⁴*CAS Key Laboratory of Theoretical Physics, Institute of Theoretical Physics,*

Chinese Academy of Sciences, Beijing 100190, China

⁵*School of Physical Sciences, University of Chinese Academy of Sciences, No. 19A Yuquan Road, Beijing 100049, China*

⁶*School of Fundamental Physics and Mathematical Sciences,*

Hangzhou Institute for Advanced Study, UCAS, Hangzhou 310024, China

(Dated: May 24, 2022)

Gravitational waves (GWs) from compact binary coalescences provide an independent probe of the cosmic expansion history other than electromagnetic waves. In this work, we assume the binary black holes (BBHs) detected by LIGO-Virgo-KAGRA (LVK) collaborations are of primordial origin and constrain the population parameters of primordial black holes (PBHs) and Hubble parameter $H(z)$ using 42 BBHs from third LVK GW transient catalog (GWTC-3). Three PBH mass models are considered: lognormal, power-law, and critical collapse PBH mass functions. By performing a hierarchical Bayesian population analysis, the Bayes factor strongly disfavors the power-law PBH mass function for the other two in GWTC-3. The constraints on standard Λ CDM cosmological parameters are rather weak and in agreement with current results. When combining the multi-messenger standard siren measurement from GW170817, the Hubble constant H_0 is constrained to be 69_{-8}^{+19} km s⁻¹ Mpc⁻¹ and 70_{-8}^{+26} km s⁻¹ Mpc⁻¹ at 68% confidence for the lognormal and critical collapse mass functions, respectively. Our results are comparable with those assuming the phenomenological mass models inspired by the astrophysical BH scenario.

I. INTRODUCTION

The Hubble parameter $H(z)$ is a fundamental observable in probing the cosmic expansion history and elucidating the nature of the dark energy component. The Planck [1] cosmic microwave background observations provide the hitherto most precise measurement of its present value, Hubble constant, as $H_0 = 67.36 \pm 0.54$ km s⁻¹ Mpc⁻¹, based on the Λ Cold Dark Matter (Λ CDM) cosmological model. Meanwhile, the recent local measurement by SH0ES team using the Cepheid variable calibrated Type Ia supernovae gives $H_0 = 73.30 \pm 1.04$ km s⁻¹ Mpc⁻¹[2]. It cracks at a 5.4σ level for the early and late Universe results, known as the Hubble tension, spurring intense debate of either new physics beyond Λ CDM or unaccounted-for systematics in current observations. Although both the early and late Universe solutions have been investigated extensively (see *e.g.* recent reviews [3–5]), this tension remains to be solved.

Gravitational waves (GWs) are new independent probes that have the potential to understand the inconsistency between the various measurements. GWs produced by compact binary coalescences can be standard sirens in the context of the general theory of relativity – the strain amplitude encodes an absolute distance to the source [6, 7]. Combined with the redshift informed by

electromagnetic (EM) counterparts, GW sirens provide a novel estimate of H_0 without using a distance ladder. This standard siren has been proven promising by the measurement with the joint GW-EM detections of binary neutron star merger event GW170817 [8].

Even in the absence of EM observations, GWs alone can probe the cosmic expansion history if the cosmological parameters are analyzed simultaneously with the population parameters of compact binaries. This can be achieved because cosmology determines how the observed (redshifted) masses scale with luminosity distance. This method has been applied to the third LIGO-Virgo-KAGRA (LVK) GW transient catalog (GWTC-3) [9] assuming that the masses and redshift of binary black holes (BBHs) follow some phenomenological distributions inspired by the astrophysical black hole (ABH) model [10], as well as in the prediction of Hubble constant for the third-generation observatories like the Einstein Telescope and Cosmic Explorer [11].

It has been speculated that the LVK BBHs are from primordial black holes (PBHs) [12] since the detection of the first GW event, GW150914 [13], as the mass of BBHs observed by GWs is unexpected heavier than those observed by X-rays [14–16]. PBHs are black holes that formed in the very early universe due to the collapse of primordial density perturbations [17, 18]. They can not only explain LVK BBHs [19–23], but also serve as cold dark matter (CDM) candidates. Moreover, the population properties of PBH binaries are quite different from those of ABH binaries. For instance, the merger rate of PBH binaries grows as the redshift z increases, while the

* zucheng.chen@bnu.edu.cn

† huangqg@itp.ac.cn

‡ Corresponding author: zhiqiang.you@bnu.edu.cn

merger rate of ABH binaries peaks at $z \sim 2$ and then decreases rapidly. In fact, this feature can be used to distinguish PBHs from ABHs [21].

In this work, we simultaneously infer the cosmic expansion history with the BBH population properties under the PBH scenario using GWTC-3 data release. The remainder of this paper is organized as follows. In Sec. II, we consider three different PBH mass spectra and review the merger rate density distribution of PBH binaries that is needed in the data analyses. In Sec. III, we describe the hierarchical Bayesian inference used to infer the model parameters. In Sec. IV, we present the constraints on the Hubble constant and the PBH population properties. Finally, we present our conclusions in Sec. V. Additionally, we put full posteriors for the three models with different PBH mass spectra in the Appendix.

II. PBH SCENARIO

In order to infer the PBH population parameters and cosmological parameters from the GWTC-3, one needs to work out the merger rate density distribution of PBH binaries. This section briefly reviews the PBH scenario under the assumption that PBH binaries are formed in the early Universe and are effectively randomly distributed in space [24]. Two neighboring PBHs will decouple from the background of the expanding Universe due to their gravitational attraction as long as they are close enough. The decoupling from the Hubble flow usually happens deep in the radiation-domination era [24]. The tidal force from other PBHs and matter density perturbations will provide an angular momentum to this pair of PBHs, preventing them from direct coalescence. This PBH pair will therefore form a binary. After the formation of a binary, the orbit of this system will shrink due to the GW radiation. The PBH binaries will eventually merge and potentially be detected by GW detectors, thus explaining LVK BBH events.

Given an extended PBH mass function, the merger rate density distribution for the PBH binaries has been worked out in [19] by accounting for the torques from all PBHs and linear density perturbations. The redshift-dependent comoving merger rate density in units of $M_\odot^{-2} \text{Gpc}^{-3} \text{yr}^{-1}$ takes the following form [19]

$$\begin{aligned} \mathcal{R}(m_1, m_2, z) &\approx 2.8 \cdot 10^6 \left(\frac{t(z)}{t_0}\right)^{-\frac{34}{37}} f_{\text{pbh}}^2 (0.7 f_{\text{pbh}}^2 + \sigma_{\text{eq}}^2)^{-\frac{21}{74}} \\ &\times \min\left(\frac{P(m_1)}{m_1}, \frac{P(m_2)}{m_2}\right) \left(\frac{P(m_1)}{m_1} + \frac{P(m_2)}{m_2}\right) \\ &\times (m_1 m_2)^{\frac{3}{37}} (m_1 + m_2)^{\frac{36}{37}}, \end{aligned} \quad (1)$$

where the component masses m_1 and m_2 are in units of M_\odot , $t(z)$ is the cosmic time at redshift z , and $t_0 \equiv t(0)$. Here, f_{pbh} is the abundance of PBH in CDM, and σ_{eq}^2 is the variance of density perturbations of the rest of dark

matter at radiation-matter equality, with $\sigma_{\text{eq}} \approx 0.005$ [24]. In this work, we use the units in which the speed of light $c = 1$. Note that the redshift evolution of the merger rate of PBH binaries follows a power-law form as $(t(z)/t_0)^{-34/37}$, which is quite different from that of astrophysical black hole (ABH) binaries and can be used to distinguish between PBHs and ABHs [21]. In Eq. (1), the PBH mass function $P(m)$ has been normalized to unity, namely

$$\int_0^\infty P(m) dm = 1. \quad (2)$$

In the following, we will consider three types of PBH mass distributions originating from different PBH formation models.

The first one is the lognormal mass function taking the form of [25]

$$P(m, \sigma_c, M_c) = \frac{1}{\sqrt{2\pi}\sigma_c m} \exp\left(-\frac{\ln^2(m/M_c)}{2\sigma_c^2}\right), \quad (3)$$

where M_c is the peak mass of $mP(m)$, and σ_c gives the width of the mass spectrum. The lognormal mass function is often a good approximation to a large class of extended mass distributions if PBHs are formed from a smooth symmetric peak in the inflationary power spectrum when the slow-roll approximation holds [26–28].

The second one is the power-law mass function of the form [29, 30]

$$P(m, M_{\text{min}}) = \frac{1}{2} M_{\text{min}}^{1/2} m^{-3/2} \Theta(m - M_{\text{min}}), \quad (4)$$

where M_{min} is the lower mass cut-off the mass spectrum. The power-law mass function typically results from a broad or flat spectrum of the curvature perturbations [30] during radiation dominated era [26].

The third one is the critical collapse mass function taking the form of [31–33]

$$P(m, \alpha, M_f) = \frac{\alpha^2 m^\alpha}{M_f^{1+\alpha} \Gamma(1/\alpha)} \exp(-(m/M_f)^\alpha), \quad (5)$$

where α is a universal exponent which is related to the critical collapse of radiation, and M_f is a mass scale at the order of horizon mass at the collapse epoch [31]. This mass function is supposed to be closely associated with a monochromatic power spectrum for the density fluctuations. In this case, there is an exponential upper cut-off at a mass scale of M_f , but no lower mass cut-off. Here and after, we dub it as CC mass function.

III. DATA AND METHODOLOGY

In this work, we use BBH events from the GWTC-3 [9] to jointly infer the PBH population parameters and cosmological parameters. GWTC-3 contains 90 GW candidates detected during the first three LVK observing

Parameter	Description	Prior
Merger rate evolution		
R_0	Local merger rate of PBH binaries in $\text{Gpc}^{-3} \text{yr}^{-1}$.	$\mathcal{U}(0, 200)$
Cosmological parameters		
H_0	Hubble constant in $\text{km s}^{-1} \text{Mpc}^{-1}$.	$\mathcal{U}(10, 200)$ (Wide prior) $\mathcal{U}(65, 77)$ (Restricted prior)
Ω_m	Present-day matter density of the Universe.	$\mathcal{U}(0, 1)$ (Wide prior) $\delta(0.315)$ (Restricted prior)
Lognormal PBH mass function		
M_c	Peak mass of the lognormal mass function.	$\mathcal{U}(5, 50)$
σ_c	Mass width of the lognormal mass function.	$\mathcal{U}(0.1, 2)$
Power-law PBH mass function		
M_{\min}	Lower mass cut-off of the power-law mass function.	$\mathcal{U}(3, 10)$
Critical collapse (CC) PBH mass function		
M_f	Horizon mass scale of the CC mass function.	$\mathcal{U}(5, 50)$
α	Universal exponent of the CC mass function.	$\mathcal{U}(0.5, 5)$

TABLE I. Parameters and their prior distributions used in the Bayesian parameter estimations.

runs. Following [10], we use 42 BBH candidates with network-matched filter signal-to-noise ratio larger than 11 and inverse false alarm rate higher than 4 year. A summary of their properties can be found in Table 1 of [10]. In the analyses, we use combined posterior samples obtained from the IMRPhenom [34, 35] and SEOBNR [36, 37] waveform families.

For each BBH event, GW experiments measure the luminosity distance D_L and redshifted masses $m_1^{\text{det}}, m_2^{\text{det}}$, instead of the redshift z and source masses m_1, m_2 . These quantities are related by

$$m_i = \frac{m_i^{\text{det}}}{1 + z(D_L; H_0, \Omega_m)}, \quad (6)$$

where H_0 is the Hubble constant, and Ω_m is the present-day matter density. The relation Eq. (6) can be used to probe cosmic expansion history even without resorting to the redshift information inferred from electromagnetic counterpart [38, 39] provided source mass distribution can be well characterized.

We consider the flat Λ CDM Universe in this work. The Hubble rate at redshift z is

$$H(z) = H_0 E(z), \quad (7)$$

where $H_0 \equiv h \times 100 \text{ km s}^{-1} \text{Mpc}^{-1}$ is the Hubble constant, and

$$E(z) = \sqrt{\Omega_m(1+z)^3 + (1 - \Omega_m)}. \quad (8)$$

In the above equation, we have neglected the contribution from the radiation and neutrinos as we are interested in a small redshift range. Given redshift z , one can then calculate the cosmic time t as

$$t(z) = \frac{1}{H_0} \int_z^\infty \frac{dz'}{E(z')(1+z')}, \quad (9)$$

and the luminosity distance D_L as

$$D_L(z) = \frac{(1+z)}{H_0} \int_0^z \frac{dz'}{E(z')}. \quad (10)$$

Solving the above equation yields the redshift as a function of luminosity distance, $z(D_L)$, that is needed in Eq. (10).

We use the hierarchical Bayesian inference to infer the model parameters. To do so, we rewrite the merger rate density Eq. (1) as

$$\mathcal{R}(\theta|\Phi) = R_0 p(\theta|\Phi), \quad (11)$$

where $\theta = \{m_1, m_2, z\}$ are the intrinsic GW parameters that are interesting for cosmology and unique for each event, while Φ denotes the hyper-parameters that are common to the entire population of GW sources. Concretely, $\Phi = \{H_0, \Omega_m, \sigma_c, M_c\}, \{H_0, \Omega_m, M_{\min}\}$, and $\{H_0, \Omega_m, \alpha, M_f\}$ for the cases of lognormal, power-law and CC mass function, respectively. The local merger rate R_0 in Eq. (11) is defined by

$$R_0 = \int_0^\infty \int_0^\infty \mathcal{R}(m_1, m_2, z=0|\Phi) dm_1 dm_2, \quad (12)$$

ensuring that $p(\theta|\Phi)$ is normalized to unity when $z=0$. Given R_0 and Φ , one can solve for f_{pbh} using Eq. (1) and Eq. (12). Note that $p(\theta|\Phi)$ are measured in source frame, and be converted to the detector frame by

$$p_{\text{pop}}(\theta|\Phi) = \frac{1}{1+z} \frac{dV_c}{dz} p(\theta|\Phi), \quad (13)$$

where dV_c/dz is the differential comoving volume, and the factor $1/(1+z)$ converts time increments from the source frame to the detector frame.

PBH mass model	$\log_{10} \mathcal{B}$
Lognormal	-0.02
Power-law	-0.11
CC	0.20

TABLE II. Logarithm of the Bayes factor comparing runs that adopt the same PBH mass model but different cosmologies: Wide priors versus Restricted priors.

Given the data, $\mathbf{d} = \{d_1, d_2, \dots, d_{\text{obs}}\}$, of N_{obs} GW events, we model the total number of events as an inhomogeneous Poisson process, yielding the likelihood [40–42]

$$\mathcal{L}(\mathbf{d}|R_0, \Phi) \propto R_0^{N_{\text{obs}}} e^{-R_0 \xi(\Phi)} \prod_{i=1}^{N_{\text{obs}}} \int \mathcal{L}(d_i|\theta) p_{\text{pop}}(\theta|\Phi) d\theta, \quad (14)$$

where $\mathcal{L}(d_i|\theta)$ is the individual likelihood for i th GW event that can be derived from the individual posterior by reweighing with the prior on θ , and

$$\xi(\Phi) = \int P_{\text{det}}(\theta) \pi(\theta|\Phi) d\theta \quad (15)$$

is the detection fraction that quantifies selection biases for a population with parameters Φ . Here, $P_{\text{det}}(\theta)$ is the detection probability that depends on the source parameters θ . We use the simulated signals (injections) that are available in [43] to estimate the detection fraction. In practice, it is approximated by using a Monte Carlo integral over found injections [44]

$$\xi(\Phi) \approx \frac{1}{N_{\text{inj}}} \sum_{j=1}^{N_{\text{found}}} \frac{\pi(\theta_j|\Phi)}{p_{\text{draw}}(\theta_j)}, \quad (16)$$

where N_{inj} is the total number of injections, N_{found} is the number of injections that are successfully detected, and p_{draw} is the probability distribution from which the injections are drawn. We incorporate the PBH population distribution (13) into the ICAROGW [45] to estimate the likelihood function, and use *dynesty* [46] sampler called from *Bilby* [47, 48] to search over the parameter space.

IV. RESULTS AND DISCUSSION

We use 42 detected BBHs with $\text{SNR} > 11$ to estimate the cosmological and population parameters. Similar to [10], we consider two cosmological models: (i) a general Λ CDM model with wide priors on the Hubble constant H_0 and matter density Ω_m , and (ii) a H_0 -tension model with a fixed value of $\Omega_m = 0.315$ [1] and with a restricted prior in the H_0 tension region ($H_0 \in [65, 77]$ $\text{km s}^{-1} \text{Mpc}^{-1}$). Table III summarizes the model parameters and their prior distributions used in the Bayesian parameter estimations. The posteriors for the three PBH

PBH mass model	$\log_{10} \mathcal{B}$
Lognormal	2.99
Power-law	0
CC	3.12

TABLE III. Logarithm of the Bayes factor between the different PBH mass models and the Power-law PBH mass model, for the case of a flat Λ CDM cosmology with wide priors.

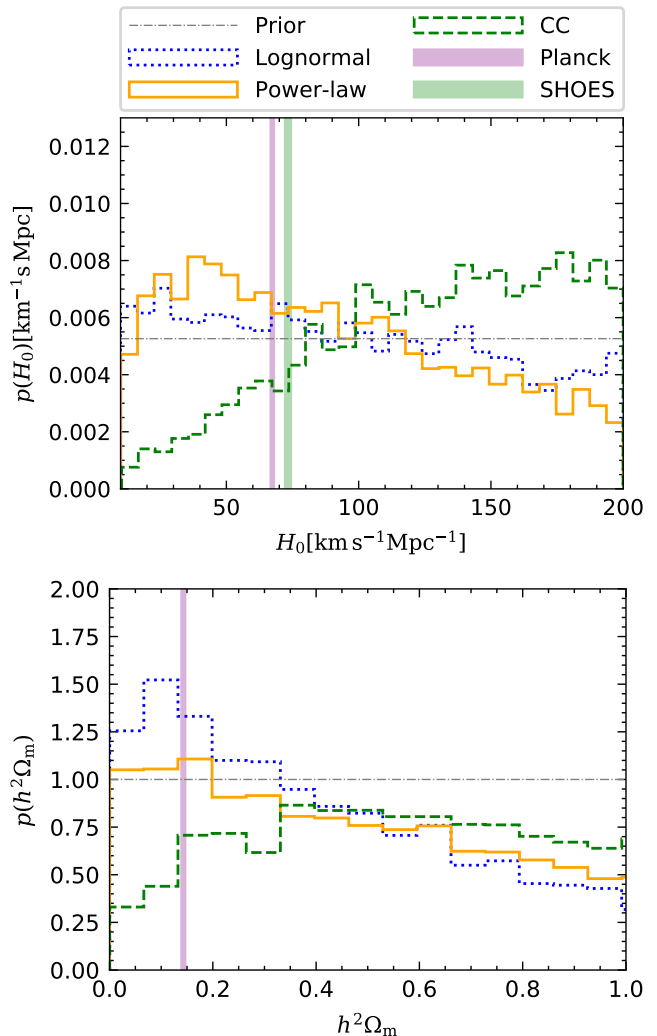


FIG. 1. *Top panel:* One-dimensional marginal posterior distribution for H_0 . *Bottom panel:* One-dimensional marginal posterior distribution for $h^2 \Omega_m$. In each panel, the blue dotted, orange solid, and green dashed lines represent the lognormal, power-law, and CC mass distributions of PBHs, respectively. The pink and green shaded areas indicate the 68% CI of the cosmological parameters inferred from CMB [1] and the local Universe measurements [2], respectively.

model models (lognormal, power-law, and CC) considered in this work are presented in Appendix.

In Table II, we report the Bayes factor between the general Λ CDM model versus the H_0 -tension model for

three different PBH mass distributions, indicating no evidence of the data in favor of any one of these two cosmological models. This is mainly because $h^2\Omega_m$ cannot be well constrained by the GW observations, and the uncertainty on the H_0 estimation extends far beyond the H_0 tension region, as can be seen from Fig. 1.

In Table III, we report the Bayes factors between different PBH mass models for the case of a general cosmology with wide priors. We find that the data strongly favor the lognormal and CC PBH mass models over the power-law model by a factor larger than ~ 1000 , but no compelling evidence to prefer the lognormal PBH mass model over the CC mass model.

Fig. 1 shows the marginal posterior distributions for the cosmological parameters H_0 and $h^2\Omega_m$ for the three different PBH mass models. The posteriors for these two cosmological parameters are broad and uninformative, indicating the current BBH events cannot constrain them, as anticipated by the Bayes factors discussed above. Fig. 2 shows the H_0 posteriors obtained by com-

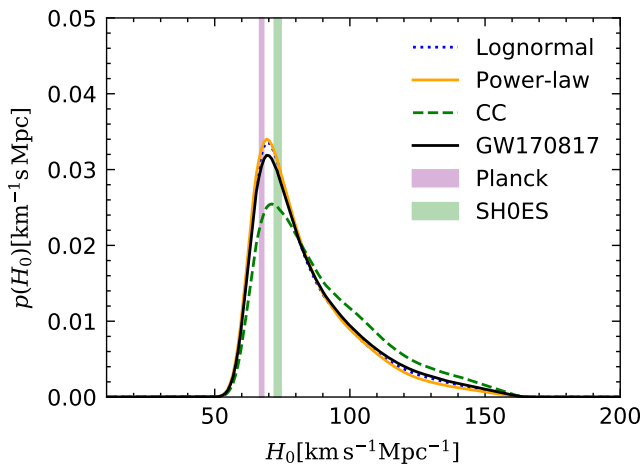


FIG. 2. One-dimensional marginal posterior distribution for H_0 obtained by combining the H_0 posteriors from the 42 BBH events and the H_0 posterior inferred from the bright standard siren GW170817. The blue dotted, orange solid, and green dashed lines represent the lognormal, power-law, and CC mass distributions of PBHs, respectively. The pink and green shaded areas indicate the 68% CI constraints on H_0 inferred from CMB [1] and the local Universe measurements [2], respectively. The H_0 posteriors for GW170817 are adapted from [10].

binning the H_0 posteriors from the three PBH mass models with the H_0 posteriors inferred from the bright standard siren GW170817 [8]. The combined estimation of the Hubble constant is $H_0 = 69_{-8}^{+19}$ km s $^{-1}$ Mpc $^{-1}$, $H_0 = 69_{-8}^{+19}$ km s $^{-1}$ Mpc $^{-1}$, and $H_0 = 70_{-8}^{+26}$ km s $^{-1}$ Mpc $^{-1}$, at the 68% credible level for the lognormal, power-law, and CC PBH mass models, respectively. Unless stated otherwise, credible intervals are quoted as maximum posterior and 68% highest density intervals. These results are at the same level compared with those obtained under

the phenomenological mass models reported in [10].

We also derive the posterior distribution for the f_{pbh} parameter. The results are shown in Fig. 3, with $f_{\text{pbh}} = 4.1_{-0.8}^{+0.5} \times 10^{-3}$, $f_{\text{pbh}} = 6.8_{-1.0}^{+1.2} \times 10^{-3}$, and $f_{\text{pbh}} = 3.7_{-0.5}^{+0.4} \times 10^{-3}$ for the lognormal, power-law, and CC PBH mass models, respectively.

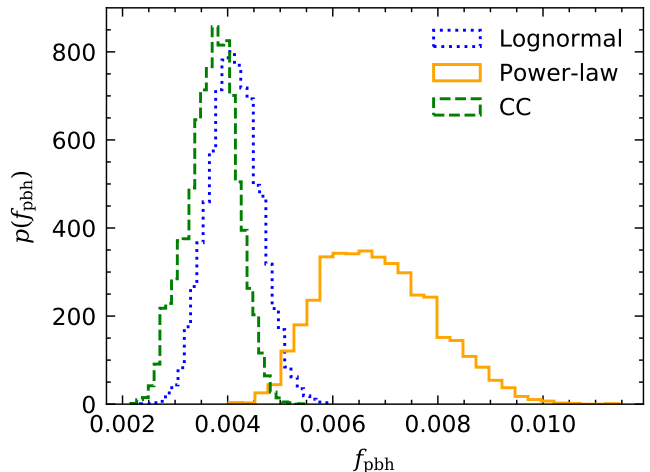


FIG. 3. One-dimensional marginal posterior distribution for the abundance of PBHs in CDM, f_{pbh} . The blue dotted, orange solid, and green dashed lines represent the lognormal, power-law, and CC mass distributions of PBHs, respectively.

V. CONCLUSION

In this work, we constrain the Hubble parameter using the 42 BBHs with detected SNR > 11 in the LVK GWTC-3 data release by assuming these BBHs are from PBHs. Three different PBH mass models are considered in the analyses. By simultaneously inferring the population parameters and the cosmological parameters, we find the data strongly disfavor the power-law PBH mass model, but no compelling evidence to prefer the lognormal PBH mass model over the CC mass model or vice versa. The abundance of PBH in CDM, f_{pbh} , is at the order $\mathcal{O}(10^{-3})$ for all three PBH mass models, confirming that the stellar-mass PBHs cannot dominate CDM.

While the constraints on the present-day matter density, Ω_m is weak and uninformative, we estimate the Hubble constant to be $H_0 = 69_{-8}^{+19}$ km s $^{-1}$ Mpc $^{-1}$ and $H_0 = 70_{-8}^{+26}$ km s $^{-1}$ Mpc $^{-1}$ at 68% confidence level for the lognormal and critical collapse mass functions, respectively, by combining the measurement from GW170817 and its EM counterpart [8]. These results are at the same level compared with those obtained under the phenomenological mass models reported in [10].

ACKNOWLEDGMENTS

We thank Xing-Jiang Zhu, Xiao-Jin Liu and Zhu Yi for useful discussions. QGH is supported by the National Key Research and Development Program of China Grant No.2020YFC2201502, grants from NSFC (grant No. 11975019, 11991052, 12047503), Key Research Program of Frontier Sciences, CAS, Grant NO. ZDBS-LY-7009, CAS Project for Young Scientists in Basic Research YSBR-006, the Key Research Program of the Chinese Academy of Sciences (Grant NO. XDPB15). This research has made use of data or software obtained from the Gravitational Wave Open Science Center (gw-openscience.org), a service of LIGO Laboratory, the LIGO Scientific Collaboration, the Virgo Collaboration, and KAGRA. LIGO Laboratory and Advanced LIGO are funded by the United States National Science Foundation (NSF) as well as the Science and Technology Facilities Council (STFC) of the United King-

dom, the Max-Planck-Society (MPS), and the State of Niedersachsen/Germany for support of the construction of Advanced LIGO and construction and operation of the GEO600 detector. Additional support for Advanced LIGO was provided by the Australian Research Council. Virgo is funded, through the European Gravitational Observatory (EGO), by the French Centre National de Recherche Scientifique (CNRS), the Italian Istituto Nazionale di Fisica Nucleare (INFN) and the Dutch Nikhef, with contributions by institutions from Belgium, Germany, Greece, Hungary, Ireland, Japan, Monaco, Poland, Portugal, Spain. The construction and operation of KAGRA are funded by Ministry of Education, Culture, Sports, Science and Technology (MEXT), and Japan Society for the Promotion of Science (JSPS), National Research Foundation (NRF) and Ministry of Science and ICT (MSIT) in Korea, Academia Sinica (AS) and the Ministry of Science and Technology (MoST) in Taiwan.

-
- [1] N. Aghanim *et al.* (Planck), “Planck 2018 results. VI. Cosmological parameters,” *Astron. Astrophys.* **641**, A6 (2020), [Erratum: *Astron. Astrophys.* 652, C4 (2021)], [arXiv:1807.06209 \[astro-ph.CO\]](#).
- [2] Adam G. Riess *et al.*, “A Comprehensive Measurement of the Local Value of the Hubble Constant with 1 km/s/Mpc Uncertainty from the Hubble Space Telescope and the SH0ES Team,” (2021), [arXiv:2112.04510 \[astro-ph.CO\]](#).
- [3] Paul Shah, Pablo Lemos, and Ofer Lahav, “A buyer’s guide to the Hubble constant,” *Astron. Astrophys. Rev.* **29**, 9 (2021), [arXiv:2109.01161 \[astro-ph.CO\]](#).
- [4] Eleonora Di Valentino, Olga Mena, Supriya Pan, Luca Visinelli, Weiqiang Yang, Alessandro Melchiorri, David F. Mota, Adam G. Riess, and Joseph Silk, “In the realm of the Hubble tension—a review of solutions,” *Class. Quant. Grav.* **38**, 153001 (2021), [arXiv:2103.01183 \[astro-ph.CO\]](#).
- [5] Leandros Perivolaropoulos and Foteini Skara, “Challenges for Λ CDM: An update,” (2021), [arXiv:2105.05208 \[astro-ph.CO\]](#).
- [6] Bernard F. Schutz, “Determining the Hubble Constant from Gravitational Wave Observations,” *Nature* **323**, 310–311 (1986).
- [7] Daniel E. Holz and Scott A. Hughes, “Using gravitational-wave standard sirens,” *Astrophys. J.* **629**, 15–22 (2005), [arXiv:astro-ph/0504616](#).
- [8] B. P. Abbott *et al.* (LIGO Scientific, Virgo, 1M2H, Dark Energy Camera GW-E, DES, DLT40, Las Cumbres Observatory, VINROUGE, MASTER), “A gravitational-wave standard siren measurement of the Hubble constant,” *Nature* **551**, 85–88 (2017), [arXiv:1710.05835 \[astro-ph.CO\]](#).
- [9] R. Abbott *et al.* (LIGO Scientific, VIRGO, KAGRA), “GWTC-3: Compact Binary Coalescences Observed by LIGO and Virgo During the Second Part of the Third Observing Run,” (2021), [arXiv:2111.03606 \[gr-qc\]](#).
- [10] R. Abbott *et al.* (LIGO Scientific, VIRGO, KAGRA), “Constraints on the cosmic expansion history from GWTC-3,” (2021), [arXiv:2111.03604 \[astro-ph.CO\]](#).
- [11] Zhi-Qiang You, Xing-Jiang Zhu, Gregory Ashton, Eric Thrane, and Zong-Hong Zhu, “Standard-siren cosmology using gravitational waves from binary black holes,” *Astrophys. J.* **908**, 215 (2021), [arXiv:2004.00036 \[astro-ph.CO\]](#).
- [12] Misao Sasaki, Teruaki Suyama, Takahiro Tanaka, and Shuichiro Yokoyama, “Primordial Black Hole Scenario for the Gravitational-Wave Event GW150914,” *Phys. Rev. Lett.* **117**, 061101 (2016), [Erratum: *Phys. Rev. Lett.* 121, 059901 (2018)], [arXiv:1603.08338 \[astro-ph.CO\]](#).
- [13] B. P. Abbott *et al.* (LIGO Scientific, Virgo), “Observation of Gravitational Waves from a Binary Black Hole Merger,” *Phys. Rev. Lett.* **116**, 061102 (2016), [arXiv:1602.03837 \[gr-qc\]](#).
- [14] Grzegorz Wiktorowicz, Krzysztof Belczynski, and Thomas J. Maccarone, “Black Hole X-ray Transients: The Formation Puzzle,” (2013), [arXiv:1312.5924 \[astro-ph.HE\]](#).
- [15] J. Casares and P. G. Jonker, “Mass Measurements of Stellar and Intermediate Mass Black-Holes,” *Space Sci. Rev.* **183**, 223–252 (2014), [arXiv:1311.5118 \[astro-ph.HE\]](#).
- [16] J. M. Corral-Santana, J. Casares, T. Muñoz-Darias, P. Rodríguez-Gil, T. Shahbaz, M. A. P. Torres, C. Zurita, and A. A. Tyndall, “A Black Hole Nova Obscured by an Inner Disk Torus,” *Science* **339**, 1048–1051 (2013), [arXiv:1303.0034 \[astro-ph.GA\]](#).
- [17] Stephen Hawking, “Gravitationally collapsed objects of very low mass,” *Mon. Not. Roy. Astron. Soc.* **152**, 75 (1971).
- [18] Bernard J. Carr and S. W. Hawking, “Black holes in the early Universe,” *Mon. Not. Roy. Astron. Soc.* **168**, 399–415 (1974).
- [19] Zu-Cheng Chen and Qing-Guo Huang, “Merger Rate Distribution of Primordial-Black-Hole Binaries,” *Astrophys. J.* **864**, 61 (2018), [arXiv:1801.10327 \[astro-ph.CO\]](#).

- [20] Zu-Cheng Chen, Fan Huang, and Qing-Guo Huang, “Stochastic Gravitational-wave Background from Binary Black Holes and Binary Neutron Stars and Implications for LISA,” *Astrophys. J.* **871**, 97 (2019), [arXiv:1809.10360 \[gr-qc\]](#).
- [21] Zu-Cheng Chen and Qing-Guo Huang, “Distinguishing Primordial Black Holes from Astrophysical Black Holes by Einstein Telescope and Cosmic Explorer,” *JCAP* **08**, 039 (2020), [arXiv:1904.02396 \[astro-ph.CO\]](#).
- [22] You Wu, “Merger history of primordial black-hole binaries,” *Phys. Rev. D* **101**, 083008 (2020), [arXiv:2001.03833 \[astro-ph.CO\]](#).
- [23] Zu-Cheng Chen, Chen Yuan, and Qing-Guo Huang, “Confronting the primordial black hole scenario with the gravitational-wave events detected by LIGO-Virgo,” *Phys. Lett. B* **829**, 137040 (2022), [arXiv:2108.11740 \[astro-ph.CO\]](#).
- [24] Yacine Ali-Haïmoud, Ely D. Kovetz, and Marc Kamionkowski, “Merger rate of primordial black-hole binaries,” *Phys. Rev. D* **96**, 123523 (2017), [arXiv:1709.06576 \[astro-ph.CO\]](#).
- [25] Alexandre Dolgov and Joseph Silk, “Baryon isocurvature fluctuations at small scales and baryonic dark matter,” *Phys. Rev. D* **47**, 4244–4255 (1993).
- [26] Bernard Carr, Martti Raidal, Tommi Tenkanen, Ville Vaskonen, and Hardi Veermäe, “Primordial black hole constraints for extended mass functions,” *Phys. Rev. D* **96**, 023514 (2017), [arXiv:1705.05567 \[astro-ph.CO\]](#).
- [27] Anne M. Green, “Microlensing and dynamical constraints on primordial black hole dark matter with an extended mass function,” *Phys. Rev. D* **94**, 063530 (2016), [arXiv:1609.01143 \[astro-ph.CO\]](#).
- [28] Kristjan Kannike, Luca Marzola, Martti Raidal, and Hardi Veermäe, “Single Field Double Inflation and Primordial Black Holes,” *JCAP* **09**, 020 (2017), [arXiv:1705.06225 \[astro-ph.CO\]](#).
- [29] Bernard J. Carr, “The Primordial black hole mass spectrum,” *Astrophys. J.* **201**, 1–19 (1975).
- [30] V. De Luca, G. Franciolini, and A. Riotto, “On the Primordial Black Hole Mass Function for Broad Spectra,” *Phys. Lett. B* **807**, 135550 (2020), [arXiv:2001.04371 \[astro-ph.CO\]](#).
- [31] B. J. Carr, Kazunori Kohri, Yuuiti Sendouda, and Jun’ichi Yokoyama, “Constraints on primordial black holes from the Galactic gamma-ray background,” *Phys. Rev. D* **94**, 044029 (2016), [arXiv:1604.05349 \[astro-ph.CO\]](#).
- [32] Jens C. Niemeyer and K. Jedamzik, “Near-critical gravitational collapse and the initial mass function of primordial black holes,” *Phys. Rev. Lett.* **80**, 5481–5484 (1998), [arXiv:astro-ph/9709072](#).
- [33] Jun’ichi Yokoyama, “Cosmological constraints on primordial black holes produced in the near critical gravitational collapse,” *Phys. Rev. D* **58**, 107502 (1998), [arXiv:gr-qc/9804041](#).
- [34] Jonathan E. Thompson, Edward Fauchon-Jones, Sebastian Khan, Elisa Nitoglia, Francesco Pannarale, Tim Dietrich, and Mark Hannam, “Modeling the gravitational wave signature of neutron star black hole coalescences,” *Phys. Rev. D* **101**, 124059 (2020), [arXiv:2002.08383 \[gr-qc\]](#).
- [35] Geraint Pratten *et al.*, “Computationally efficient models for the dominant and subdominant harmonic modes of precessing binary black holes,” *Phys. Rev. D* **103**, 104056 (2021), [arXiv:2004.06503 \[gr-qc\]](#).
- [36] Serguei Ossokine *et al.*, “Multipolar Effective-One-Body Waveforms for Precessing Binary Black Holes: Construction and Validation,” *Phys. Rev. D* **102**, 044055 (2020), [arXiv:2004.09442 \[gr-qc\]](#).
- [37] Andrew Matas *et al.*, “Aligned-spin neutron-star–black-hole waveform model based on the effective-one-body approach and numerical-relativity simulations,” *Phys. Rev. D* **102**, 043023 (2020), [arXiv:2004.10001 \[gr-qc\]](#).
- [38] Stephen R. Taylor, Jonathan R. Gair, and Ilya Mandel, “Hubble without the Hubble: Cosmology using advanced gravitational-wave detectors alone,” *Phys. Rev. D* **85**, 023535 (2012), [arXiv:1108.5161 \[gr-qc\]](#).
- [39] Stephen R. Taylor and Jonathan R. Gair, “Cosmology with the lights off: standard sirens in the Einstein Telescope era,” *Phys. Rev. D* **86**, 023502 (2012), [arXiv:1204.6739 \[astro-ph.CO\]](#).
- [40] Thomas J. Loredo, “Accounting for source uncertainties in analyses of astronomical survey data,” *AIP Conf. Proc.* **735**, 195–206 (2004), [arXiv:astro-ph/0409387](#).
- [41] Eric Thrane and Colm Talbot, “An introduction to Bayesian inference in gravitational-wave astronomy: parameter estimation, model selection, and hierarchical models,” *Publ. Astron. Soc. Austral.* **36**, e010 (2019), [Erratum: *Publ. Astron. Soc. Austral.* **37**, e036 (2020)], [arXiv:1809.02293 \[astro-ph.IM\]](#).
- [42] Ilya Mandel, Will M. Farr, and Jonathan R. Gair, “Extracting distribution parameters from multiple uncertain observations with selection biases,” *Mon. Not. Roy. Astron. Soc.* **486**, 1086–1093 (2019), [arXiv:1809.02063 \[physics.data-an\]](#).
- [43] LIGO Scientific Collaboration, Virgo Collaboration, and KAGRA Collaboration, “GWTC-3: Compact Binary Coalescences Observed by LIGO and Virgo During the Second Part of the Third Observing Run — O3 search sensitivity estimates,” (2021), <https://doi.org/10.5281/zenodo.5546676>.
- [44] R. Abbott *et al.* (LIGO Scientific, VIRGO, KAGRA), “The population of merging compact binaries inferred using gravitational waves through GWTC-3,” (2021), [arXiv:2111.03634 \[astro-ph.HE\]](#).
- [45] S. Mastroianni, K. Leyde, C. Karathanasis, E. Chassande-Mottin, D. A. Steer, J. Gair, A. Ghosh, R. Gray, S. Mukherjee, and S. Rinaldi, “On the importance of source population models for gravitational-wave cosmology,” *Phys. Rev. D* **104**, 062009 (2021), [arXiv:2103.14663 \[gr-qc\]](#).
- [46] Joshua S. Speagle, “dynesty: a dynamic nested sampling package for estimating Bayesian posteriors and evidences,” *Mon. Not. Roy. Astron. Soc.* **493**, 3132–3158 (2020), [arXiv:1904.02180 \[astro-ph.IM\]](#).
- [47] Gregory Ashton *et al.*, “BILBY: A user-friendly Bayesian inference library for gravitational-wave astronomy,” *Astrophys. J. Suppl.* **241**, 27 (2019), [arXiv:1811.02042 \[astro-ph.IM\]](#).
- [48] I. M. Romero-Shaw *et al.*, “Bayesian inference for compact binary coalescences with bilby: validation and application to the first LIGO–Virgo gravitational-wave transient catalogue,” *Mon. Not. Roy. Astron. Soc.* **499**, 3295–3319 (2020), [arXiv:2006.00714 \[astro-ph.IM\]](#).
- [49] Daniel Foreman-Mackey, “corner.py: Scatterplot matrices in python,” *The Journal of Open Source Software* **1**, 24 (2016).

Appendix: posteriors

In this appendix, we show the posteriors of all the cosmological parameters and population parameters for the three different mass models considered in our analyses. The corner plots are produced using the `corner` [49] package.

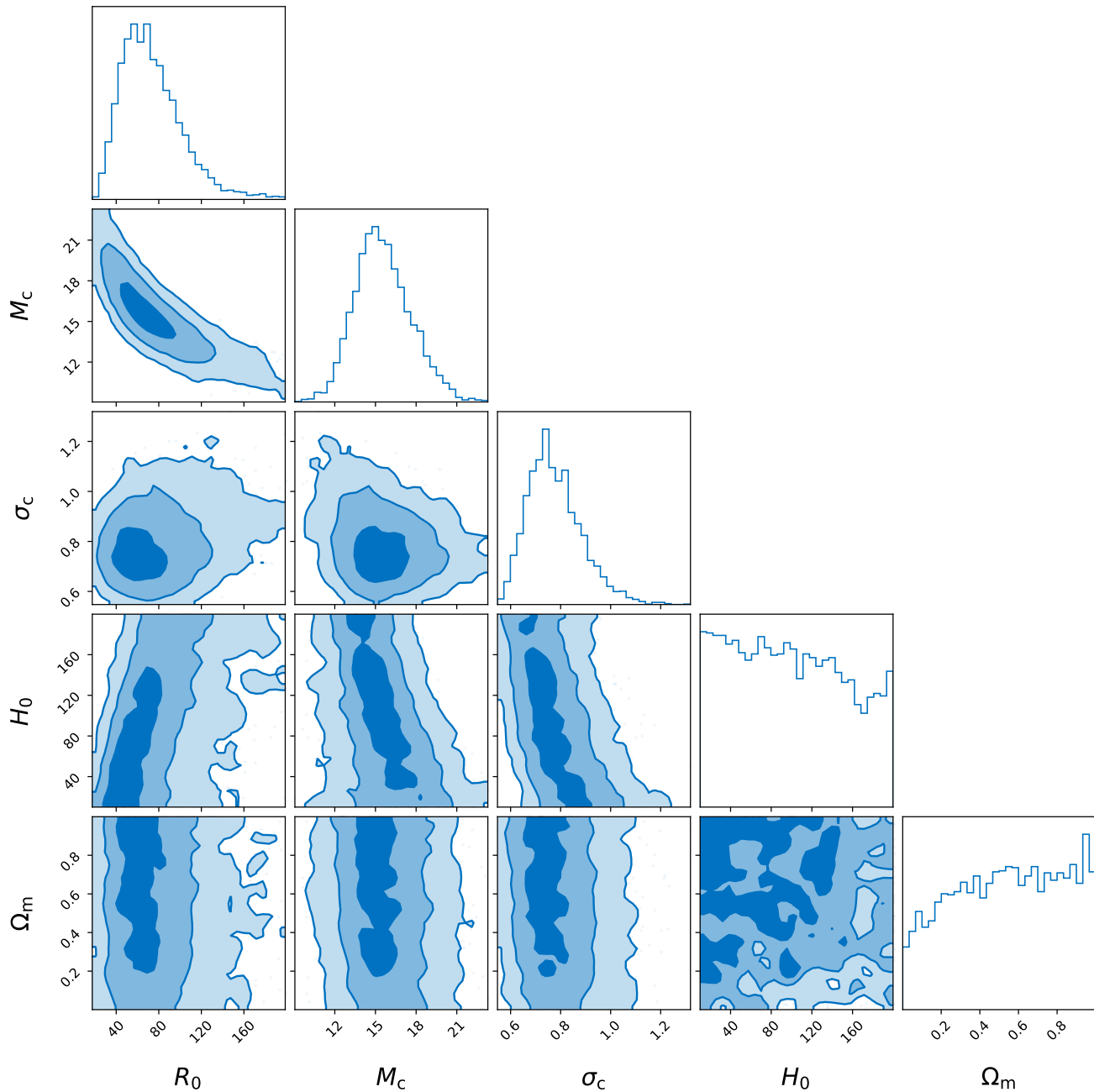


FIG. 4. One and two-dimensional marginalized posteriors of the hyper parameters for the lognormal mass distribution. We show both the 1σ , 2σ , and 3σ contours in the two-dimensional plot.

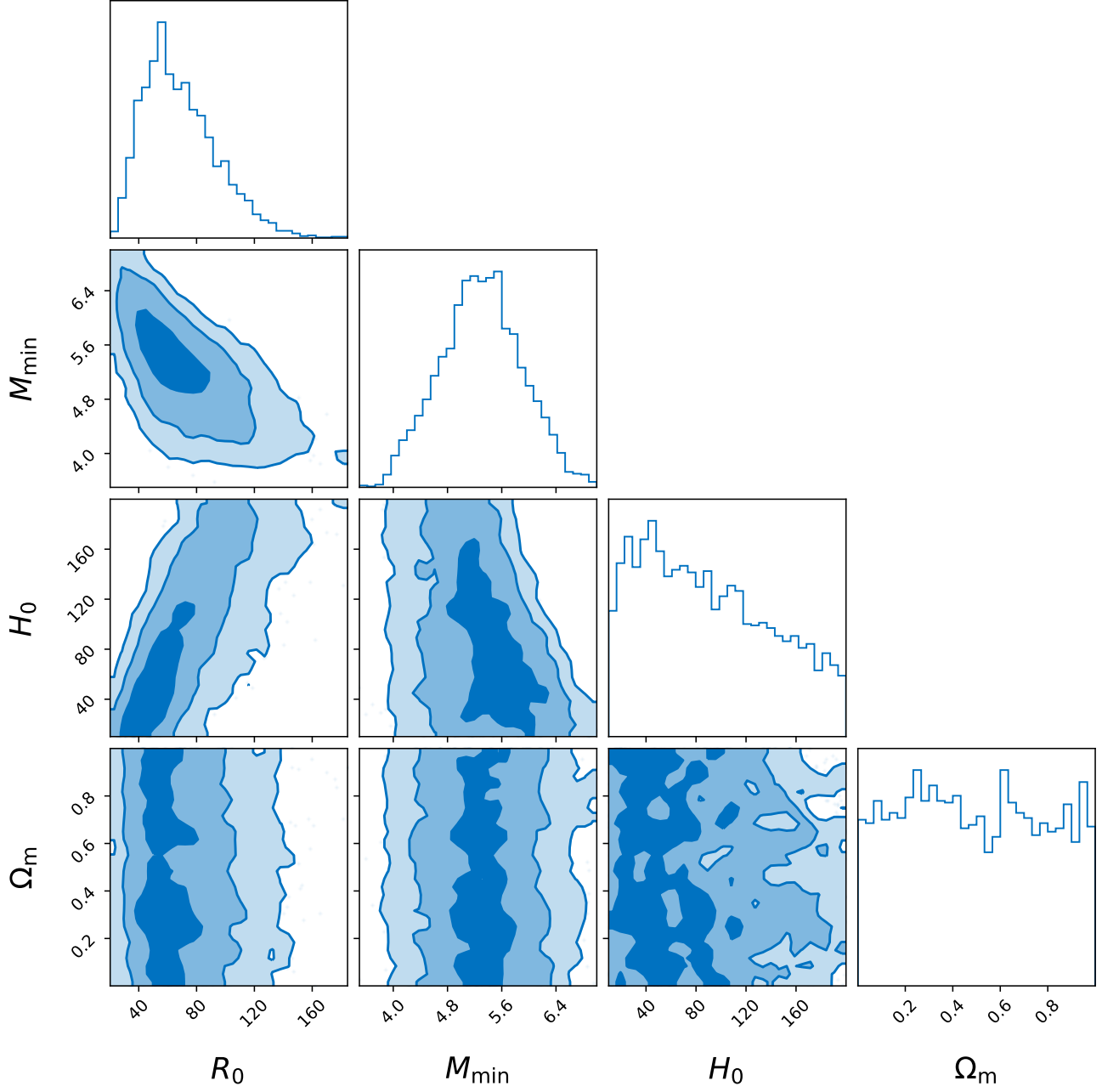


FIG. 5. One and two-dimensional marginalized posteriors of the hyper parameters for the powerlaw mass distribution. We show both the 1σ , 2σ , and 3σ contours in the two-dimensional plot.

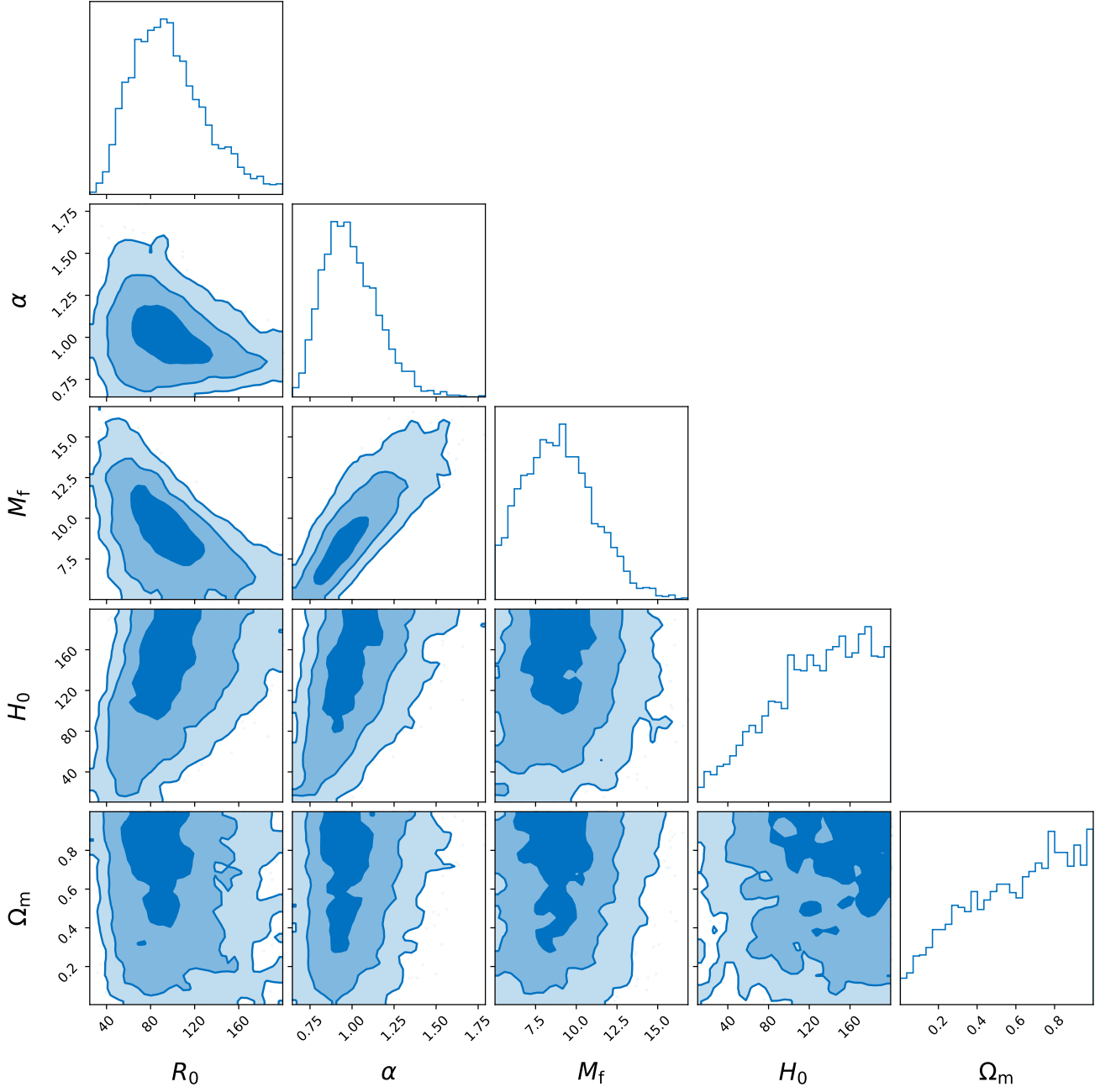


FIG. 6. One and two-dimensional marginalized posteriors of the hyper parameters for the CC mass distribution. We show both the 1σ , 2σ , and 3σ contours in the two-dimensional plot.